# Numerical Simulations of Axisymmetric Flows
# in Astrophysics and their Visualization
# by a Video Movie

### By

Takuya MATSUDA*, Hiroshi KOIDE*, Yuzo FUJIMOTO*, Nobuhiro SEKINO*
Keisuke SAWADA** and Eiji SHIMA**
(Received March 31, 1989)

### Abstract

Numerical simulations of axisymmetric flow in four different astrophysical situa-
tions are performed, and their results are visualized by using a video movie. The situa-
tions considered are : 1) an accretion flow on to a gravitating compact object allowing
maximum accrection ; 2) a jet formation in a flow past a gravitating rigid sphere ; 3) an
interaction between a supersonic wind from a central object and a uniform supersonic
incident flow ; 4) a wind bubble formed by spherical supersonic wind. The video tape
of VHS/NTSC format is available from the author.

## 1. Numerical method

The method of calculation is an implicit Osher upwind scheme with the second-
order of space accuracy. The accuracy in time integration is the first-order. The detail
of the Osher scheme was described by Sawada et al. (1986), and that of the time integra-
tion was given by Matsuda et al. (1987).

The polar grid was used in all calculations except the case of the wind interaction,
where an O-type generalized curvilinear coordinate was used.

The computations were performed on the Fujitsu VP400E or VP200 vector proces-
sor at the Data Processing Center of Kyoto University. The theoretical maximum speed
of VP400E is 1.7GFLOPS and that of VP200 is 0.6 GFLOPS. However, in terms of a
sustained speed VP400E is only 20-30 percent faster than VP200 in our code. The main
memory of VP400E is 256MB, while that of VP200 is 64MB.

---

\*     Department of Aeronautical Engineering
\*\*    Aerospace Engineering Division, Kawasaki Heavy Industries Ltd.,

## 2. An axisymmetric accretion flow on to a compact object

This problem was investigated by Shima et al. (1985) earlier, and recently it was fully investigated by Ho et al. (1988). The present video shows some of the results by Ho et al.

A gravitating spherical body is immeresed in a uniform incident flow. The body is assumed to be a hollow sphere, in which negligible pressure and density are specified to allow a maximum accretion. The ratio of the specific heats is fixed to be

$$\gamma = \frac{5}{3}. \tag{1}$$

The Hoyle-Lyttleton accretion radius $r_A$ is defined as

$$r_A = \frac{2Gm}{V^2}, \tag{2}$$

where $m$ and $V$ are the mass of the body and the velocity of gas at the far-upstream, respectively. We define the ratio of the accretion radius to the radius of the central body as $\delta$. In the present case

$$\delta = 66. \tag{3}$$

Two cases of upstream Mach number $M$ are shown

$$M = 5 \; and \; 10. \tag{4}$$

The number of grid points is 106 in the radial direction and 65 in the azimuthal direction. The outer boundary is placed at $5r_A$, where a uniform incident flow is assumed.

### 2. 1 Mach number contour of the case, $M=5$

The first motion picture shows the time evolution of the Mach number contours in the case of $M=5$. Here, the red color shows the lower Mach number while the blue color shows the higher Mach number. The flow is from left to right. Only the upper half is shown.

One should note the motion of the stagnation point on the symmetry axis. It moves slowly from downstream (right) to upstream (left) before it settles about at $z = 1.1$, where $z$ is the symmetry axis and the unit of length is $r_A$. The merging of the off-axis stagnation point (ring) and the on-axis stagnation point is interesting to note.

Another interesting feature is the oscillation of the bow shock. This phenomenon is best seen in the particle motion shown later.

### 2. 2 Mach number contour of the case, $M=10$

This shows the same picture as 2.1, except $M = 10$. One can see that two off-axis stagnation points move to merge with the on-axis one, which finally settle about $z = 1.1$.

Fig. 1 shows the final stage. Only the upper half of the computational domain is shown. The oscillation of the bow shock is more amplified than the cases of the lower Mach number.

### 2. 3  Streak lines of the case, $M = 10$

In order to see the motion of the fluid elements clearly, we present the time evolution of the streak lines. At the left end of the picture, marker particles are introduced, and their motions are followed based on the calculated results. Near the stagnation point a large dead-air zone is developed, and marker particles do not get into the zone.

One can also clearly see the cause of the osciallatory motion of the bow shock. The particles which miss the central target go ahead of the body to form a small vortex. It is washed down by the ram pressure of the incident flow, and a quasi-periodic motion is excited. This phenomenon is more pronounced if the body does not accrete mass as will be discuss later.

Another feature to be noticed is the wavy motion of the streak lines behind the bow shock. This is probably caused by the Kelvin-Helmoltz instability of the flow. The 2D planar calculations by Anzer et al. (1987) show this phenomenon clearly. Considering these, it is unlikely that an axisymmetric accretion flow is completely steady.

### 2. 4  Time lines of the case, $M = 10$

In the above picture the fluid motion in the dead-air zone is difficult to observe. In order to see this, we present the behavior of the time lines, which are trajectories of the marker particles injected into the computational region periodically on the straight line at the left end.


### 3.  Flow past a gravitating rigid sphere


It is not well understood how effectively a compact star accretes mass. Therefore, it would be worthwhile to investigate the opposite extreme case, i. e. no accretion at all. We present here the flow past a gravitating rigid sphere with a refractory boundary condition. Such a flow was investigated by Shima et al. (1985) and was found to be very unsteady. Fryxell et al. (1987) investigated the case fully and found that a twin jet was formed along the symmetry axis.

Matsuda et al. (1989a) concentrated on the case of $M = 1.4$ and confirmed Fryxell et al's results generally. The cause of the jet formation is best understood by observing the motion pictures. We restricted ourselves to the case of

$$M = 1.4 \ and \ \delta = 40. \tag{5}$$

### 3. 1  Vorticity contours

Since gas is not absorbed by the body, an atmosphere is formed about the body.

An interaction between the atmosphere and the incident flow results in circulations or vortex rings in the atmosphere. In order to see this, the vorticity contours are presented. Fig. 2 shows a snapshot, in which the incident flow is from the left. The blue color shows the eddies rotating clockwise in the upper-half plane, while the red color shows the counterclockwise ones. The left-hand side is the upstream, and one can see the bow shock.

One can see that the vortices are constantly generated near the body. A part of the vortex ring overshoots to form a jet, which rolls up by the Kelvin-Helmholtz instability and finally is washed down by the incident flow. This is best observed in the following streak lines.

In order to see the effect of the boundary condition on the central body, the boundary condition is switched to that of the maximum absorption at some instance. The whole flow suddenly changes to a very steady accretion flow. After some time, the boundary condition swiches back to the original one, and we obtain a violent flow again.

## 3. 2 Streak lines

The time development of the streak lines about a gravitating rigid sphere is shown in the present motion picture. One can clearly see the vortex motion and the jet formation both along the front axis and the rear axis.

## 4. Interaction between supersonic stellar wind and the ambient flow

Suppose an astronomical object emitting supersonic spherical wind is immeresed in a uniform supersonic flow. We neglect gravity in this case in order to make the problem simple. A very complicated flow structure is expected. This problem was investigated by Shima et al. (1986) and Inaguchi et al. (1986), including gravity. Here, we repeat the calculation using a much finer grid to show the Kelvin-Helmholtz instability (Matsuda et al., 1989b).

The Mach number of the incident flow is fixed to be

$$M=15. \tag{6}$$

There are four kinds of discontinuities in the flow : 1) a bow shock or an outer shock, 2) a contact surface separating the shocked incident flow from the shocked stellar wind, 3) a bullet shaped inner shock, and 4) a slip surface originating from the corner of the Mach disc, which is the planer part of the inner shock.

In order to obtain the solution, we first compute the flow on a coarser grid., In this case we obtain a steady flow because of a bigger numerical viscosity. Then, we swiched to a finer grid having $129 \times 129$ mesh points to simulate the Kelvin-Helmholtz instability.

In the video, the time evolution of entropy contours is shown. Fig. 3 shows its

snapshot. The incident flow is from left to right. The blue color at the outer region shows an unpertubed incident flow, while the inner blue one shows the unperturbed stellar wind. The boundaries bordering these blue regions are the outer and the inner shock, respectively.

One can clealy observe the Kelvin-Helmholtz roll-up on the contact surface. The K-H waves seem to originate near the head of the contact surface.

Another interesting feature is the change of the shape of the inner shock. A corner on the inner shock propagates downstream. When it reaches the Mach disc, shock waves seem to be generated, and they propagate downstream in the downstream jet. These shocks are shown as red spots along the rear symmetry axis.

## 5. A bubble formation due to an expanding stellar wind

If the Mach number of the incident flow is 0, we obtain a stellar wind expanding into a stagnant uniform atmosphere. This is a spherical piston problem, and we have the outer shock, the contact surface and the inner shock.

In the video the entropy contours are shown, while a snapshot of the density contours is shown in Fig. 4, the color of which is different from the video. The outer shock is very weak and it is difficult to identify it in the video. It situates almost near the outer numerical boundary in Fig. 4. The border between the red color and the blue color (in the video) or that between the blue and the yellow (in Fig. 4) is the contact surface, which expands quickly in the early phase. The border between the red color and the light green (in the video) or that between the dark blue and the blue (in Fig. 4) is the inner shock, which is almost standing. The contact surface is very disturbed at the later stage. The flow between the contact surface and the inner shock is turbulent. This is because the inner shock is converging on the rest frame of the wind, and it is ustable to perturbation. On the other hand, the outer shock is very stable and spherical.

### References

Anzer, U., Börner, G. and Monaghan, J. J., Numerical Studies of Wind Accretion., 1987, Astron. Astrophys., **176**, 235.

Fryxell, B. A., Taam, R. E. and McMillan, S. L. W., Numerical Simulations of Adiabatic Axisymmetric Flow I. A New Mechanism for the Formation of Jets., 1987, Astrophys. J., **315**, 536.

Ho, C., Taam, R. E., Fryxell, B. A., Matsuda, T., Koide, H. and Shima, E., Pressure Gradient Torque in Highly Supersonic Non-Axisymmetric Accretion., 1989, Mon. Not. R. astr. Soc., **238**, 1447.

Inaguchi, T., Matsuda, T. and Shima, E., Rocket Effect on a Gravitating Mass-Losing Object., 1986, Mon. Not. R. astr. Soc., **223**, 129.

Matsuda, T., Inoue, M., Sawada, K., Shima, E. and Wakamatsu, K., A Reinvestigation of Gas Response to an Ovally Deformed Gravitational Potential., 1987, Mon. Not. R. astr. Soc.., **229**,295.

Matsuda, T., Sekino, N., Shima, E. and Sawada K., Numerical Simulations of Axisymmetric Adiabatic Flow Past a Gravitating Solid Sphere., 1989a, Mon. Not. R. astr. Soc., **236**, 817.

Matsuda, T., Fujimoto, Y., Shima, E., Sawada, K. and Inaguchi, T., Numerical Simulations of Interaction between Stellar Wind and Interstellar Medium., 1989b, Prog. Theor. Phys., **81**, 810

Sawada, K., Shima, E., Matsuda, T. and Inaguchi, T., The Osher Upwind Scheme and its Application to Cosmic Gas Dynamics. 1989, Memoirs of the Faculty of Engineering, Kyoto University, **48**, 240.

Shima, E., Matsuda, T., Takeda, H. and Sawada, K., Hydrodynamic Calculations of Axisymmetric Accretion Flow., 1985, Mon. Not. R. astr. Soc., **217**, 367.

Shima, E., Matsuda, T. and Inaguchi, T., Interaction between a Stellar Wind and an Accretion Flow., 1986, Mon. Not. R. astr. Soc., **221**, 687.
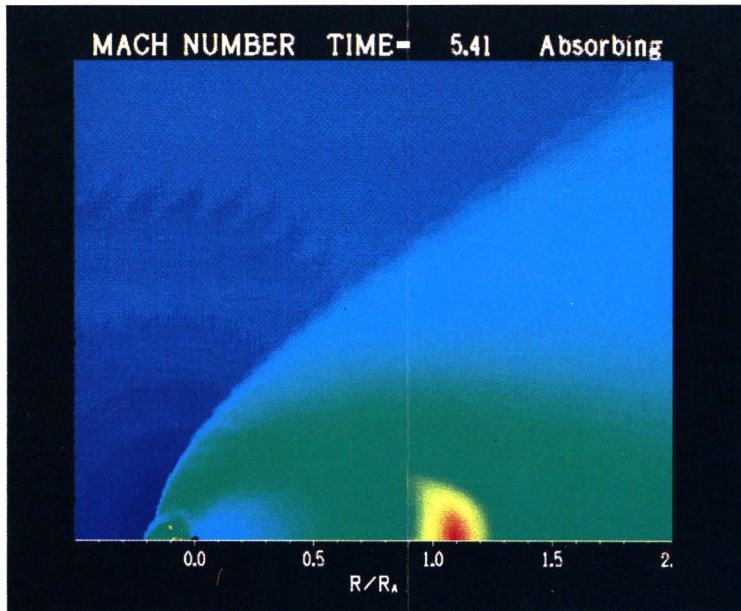
Fig. 1  Mach number contours of an axisymmetric accretion flow on to a maximally absorbing gravitating object. Only the upper half of the computational region is shown. The lower horizontal line shows the symmetry axis, and the attached number is normalized by the accretion redius. The red color shows the lower Mach number, while the blue color shows the higher one. The Mach number of the incident flow is 10.
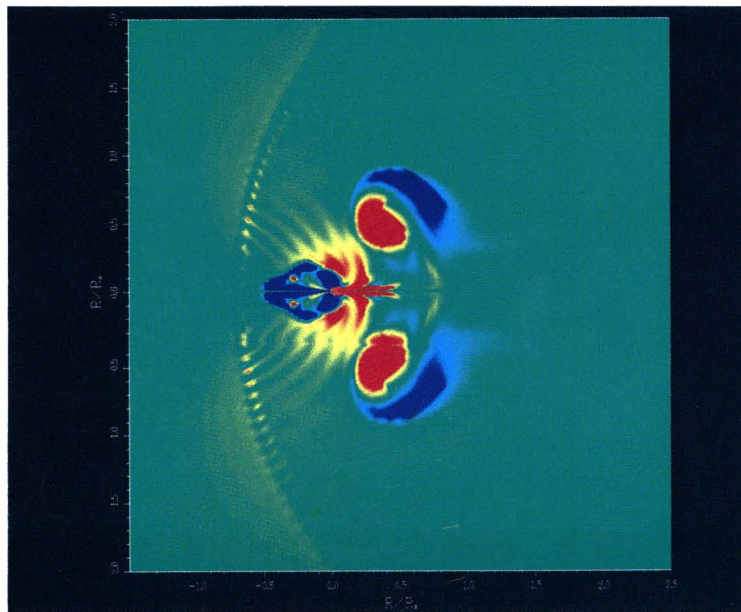


Fig. 2  Vorticity contours of an axisymmetric flow past a gravitating rigid sphere. The red color shows vortices rotating counter-clockwise in the upper-half plane. The Mach number of the incident flow is 1. 4.
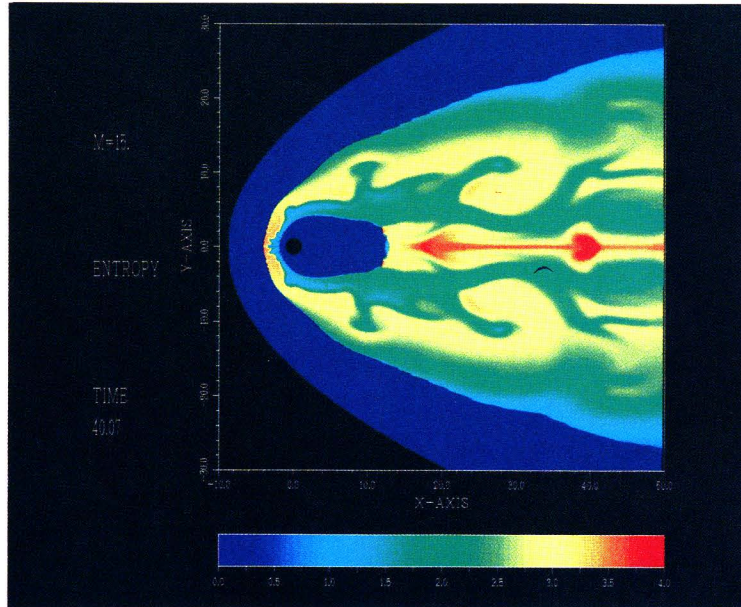
Fig. 3   Entropy contours of a supersonic spherical stellar wind immeresed in a uniform incident supersonic flow with Mach number 15. An outer shock (a bow shock), a contact surface, a bullet shaped inner shock and a slip surface can be identified.
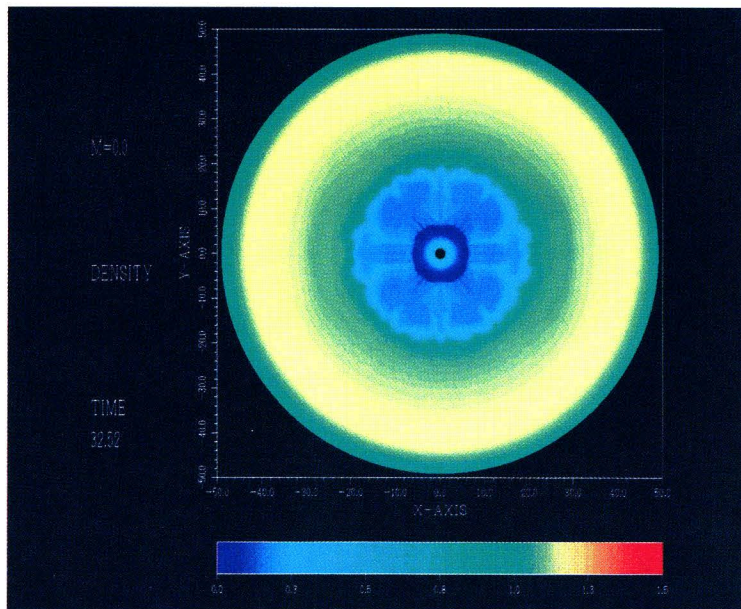


Fig. 4   Density contours of a spherical supersonic wind expanding into a stagnant uniform gas. An outer shock, a contact surface and an inner shock are identified.